

1 **Origin, evolution and dynamic context of a Neoglacial lateral-frontal**
2 **moraine at Austre Lovénbreen, Svalbard**

3 Nicholas G. Midgley^{a*}, Simon J. Cook^b, David J. Graham^c and Toby N. Tonkin^a

4

5 ^a School of Animal, Rural and Environmental Sciences, Nottingham Trent
6 University, Brackenhurst Campus, Southwell, Nottinghamshire, NG25 0QF, UK.

7

8 ^b School of Science and the Environment, Manchester Metropolitan University,
9 Chester Street, Manchester, M1 5GD, UK.

10

11 ^c Polar and Alpine Research Centre, Department of Geography, Loughborough
12 University, Leicestershire, LE11 3TU, UK.

13

14 Keywords: debris-rich basal glacier ice, ground-penetrating radar, moraine,
15 Svalbard

16

17 * Corresponding author. Tel.: +44 1636 817 016; fax: +44 1636 817 066.

18 E-mail address: nicholas.midgley@ntu.ac.uk

19

20 **Abstract**

21 Moraines marking the Neoglacial limits in Svalbard are commonly ice cored.
22 Investigating the nature of this relict ice is important because it can aid our
23 understanding of former glacier dynamics. This paper examines the
24 composition of the lateral-frontal moraine associated with the Neoglacial limit
25 at Austre Lovénbreen and assesses the likely geomorphological evolution. The
26 moraine was investigated using ground-penetrating radar (GPR), with context
27 being provided by structural mapping of the glacier based on an oblique aerial
28 image from 1936 and vertical aerial imagery from 2003. Multiple up-glacier
29 dipping reflectors and syncline structures are found in the GPR surveys. The
30 reflectors are most clearly defined in lateral positions, where the moraine is
31 substantially composed of ice. The frontal area of the moraine is dominantly
32 composed of debris. The core of the lateral part of the moraine is likely to
33 consist of stacked sequences of basal ice that have been deformed by strong
34 longitudinal compression. The long term preservation potential of the ice-
35 dominated lateral moraine is negligible, whereas the preservation of the
36 debris-dominated frontal moraine is high. A glacier surface bulge, identified on
37 the 1936 aerial imagery, provides evidence that Austre Lovénbreen has
38 previously displayed surge activity, although it is highly unlikely to do so in the
39 near future in its current state. This research shows the value of relict buried
40 ice that is preserved in landforms to aiding our understanding of former glacier
41 characteristics.

42

43 **1. Introduction**

44 The aim of this research is to investigate the origin of buried glacier ice within
45 the lateral-frontal moraine of Austre Lovénbreen, Svalbard (Fig. 1), and to
46 assess the evolution and preservation potential of this landform as the ice core
47 degrades over time. To achieve this aim, a detailed ground-penetrating radar
48 (GPR) survey was used to determine the internal architecture and composition
49 of the moraine and ice core, and set this within the structural and dynamic
50 context of the glacier by undertaking glacier structural mapping from
51 contemporary vertical aerial and historic oblique aerial imagery. The ice core
52 within the moraine preserves potentially valuable palaeoglaciological
53 information from the Neoglacial maximum, which combined with structural
54 mapping, extends recent work in the region that has examined changing
55 glacier characteristics and dynamics (Hambrey et al., 2005). Such work is
56 necessary in order to contextualise glacier change in the Arctic, a region which
57 has experienced exceptional rates of warming in recent decades (IPCC, 2007).
58 In addition, landforms at contemporary glaciers are commonly used as
59 analogues for the interpretation of mid-latitude Pleistocene glacial landforms,
60 so a fuller understanding of the formation and post-formational evolution of
61 moraines in contemporary settings such as this can also aid our understanding
62 of previously glaciated settings.

63

64 **2. Research context**

65 The lateral and frontal moraines formed at the Neoglacial maximum limits in
66 Svalbard are often considered to be ice-cored (e.g. Glasser and Hambrey,

67 2003). Lateral moraines have traditionally been considered to have formed by
68 the accumulation of thin layers of coarse angular debris on top of a thick
69 glacier ice accumulation (e.g. Flint, 1971; Embleton and King, 1975; Sugden
70 and John, 1976; Boulton and Eyles, 1979). According to this model, lateral
71 moraines have low preservation potential during deglaciation as the ice would
72 ablate quickly under a thin debris cover. The term has also been used to refer
73 to both moraines that are detached from the glacier and to thin debris covers
74 at the margins of active glacier ice. Where the debris cover in ice-cored lateral
75 moraines is both thin and contains a significant component of fine-grained
76 sediment, the debris cover is prone to reworking and exposure of the relict
77 glacier ice. Where the debris cover allows, an ice-core can form a relatively
78 stable part of the landform. Ice-cored lateral-frontal moraines have been
79 reported from a number of glaciers in Svalbard, including: Scott Turnerbreen
80 (Lønne and Lauritsen, 1996); Kongsvegen (Bennett et al., 2000);
81 Longyearbreen and Larsbreen (Etzelmüller et al., 2000; Lukas et al., 2005);
82 Rieperbreen (Lyså and Lønne, 2001); Platåbreen (Lønne and Lyså, 2005);
83 Platåbreen / Nordenskiöldtoppenbreen (Lukas et al., 2005); Holmströmbreen
84 (Schomaker and Kjær, 2008); and Ragnarbreen (Ewertowski et al., 2012).

85 The use of the term ice-cored moraine has also caused some debate with
86 Lukas et al. (2007) arguing for a strict application of the term with detachment
87 from the glacier needed to justify its application. A more pragmatic use of the
88 ice-cored moraine term has also been reasoned for (Lønne, 2007; Evans, 2009)
89 with the term not needing to indicate detachment from a glacier.

90 Evans' (2009) work on *controlled moraine* formation highlights the 'linearity'
91 that is found in landforms associated with incorporated ice. This linearity can,
92 typically, be seen on aerial images (e.g. the western end of the outer moraine
93 in Fig. 2) and serves as a useful and simple diagnostic criterion for the
94 recognition of potential ice-cored character.

95 Investigation of ice-cored moraines can potentially aid our understanding of
96 former glacier characteristics and any associated climatic significance. The ice
97 core within such moraine complexes may include glacier ice, basal ice, or a
98 combination of both. At modern ice margins, basal ice may record important
99 information about prevailing conditions and the processes operating in the
100 inaccessible subglacial environment further up-glacier (Hubbard and Sharp,
101 1989; Knight, 1997; Hubbard et al., 2009). Evidence for tectonic deformation
102 of the ice-core sequence (i.e. folds and thrusts) could also indicate a range of
103 dynamic and flow conditions when the ice was part of the parent glacier. For
104 example, englacial thrusts and folds have been inferred to indicate flow
105 compression either as a result of polythermal glacier conditions (e.g. Hambrey
106 et al., 1999), ice flow against a steep reverse bedslope (e.g. Swift et al., 2006),
107 or during glacier surges (e.g. Sharp et al., 1994; Waller et al., 2000). Some of
108 these basal ice characteristics may also be preserved in the moraine sediment
109 as the basal ice melts, offering the potential to reconstruct basal ice
110 characteristics from deglaciated terrain (e.g. Evans, 2009; Knight et al., 2000;
111 Cook et al., 2011).

112 Recent work by Hambrey et al. (2005) at neighbouring Midtre Lovénbreen
113 highlighted the value of glacier structural mapping in developing an

114 understanding of the changing dynamics of glaciers in the context of climatic
115 warming. The work of Hambrey et al. (2005) remains, however, an isolated
116 example of how analysis of temporally separated aerial and oblique aerial
117 imagery can be used to evaluate glaciological change over time. Our study
118 extends the record of changing glacier dynamics in this region, and thereby
119 contributes to a broader understanding of both glacier and climatic change in
120 the region. In particular, and as highlighted in the study of Midtre Lovénbreen,
121 there is some uncertainty about whether the Lovénbreen glaciers experience
122 surge-type behaviour (Hambrey et al., 2005). Ground-based imagery of these
123 glaciers by Hamberg (1894) from 1892 showed near-vertical ice cliffs at their
124 Neoglacial moraines. This feature was interpreted by Liestøl (1988) to indicate
125 surging. Hagen et al. (1993) also classify Midtre Lovénbreen as a surge-type
126 glacier. Later work by Jiskoot et al. (2000) indicated that these glaciers were
127 not surge-type, whereas Hansen (2003) suggested that Midtre Lovénbreen had
128 surged in the past, but could no longer be classified as a surge-type glacier. On
129 the basis of structural analysis, Hambrey et al. (2005) also concluded that
130 Midtre Lovénbreen was not a surge-type glacier, or at least had not surged for
131 several hundred years. Recognition of surge-type behaviour has important
132 implications for understanding their behaviour in the context of climatic change,
133 since glacier surges may lead to advance even during climatic amelioration.
134 Little is known about whether Austre Lovénbreen has experienced surging
135 behaviour in the past, but our analysis of historical and modern aerial imagery,
136 as well as the structures preserved within the ice-core of the Neoglacial
137 moraine, contributes to our understanding of the dynamics of this glacier.

139 3. Study area

140 Austre Lovénbreen (78°53'12''N 12°08'50''E) is located near Ny-Ålesund on
141 Brøggerhalyøva on the island of Spitsbergen, part of the Svalbard archipelago,
142 in the Norwegian high-Arctic (Fig. 1). Austre Lovénbreen is a small valley
143 glacier that was around 5 km in length at its Neoglacial maximum, but is
144 currently just less than 4 km in length.

145 The thermal regime of Austre Lovénbreen in 2010 was polythermal, based on
146 our interpretation of GPR profiles undertaken in 2010 by Saintenoy et al.
147 (2013), albeit with an extensive region of cold-based ice and an exceptionally
148 small region of warm-based ice at the deepest part of the glacier. The
149 longitudinal profile of the Austre Lovénbreen bed, again based on our
150 interpretation of GPR profiles undertaken by Saintenoy et al. (2013), also
151 highlights an overdeepening starting at around 250 m and extending to around
152 2.7 km up-glacier from the 2010 glacier terminus (Fig. 4 in Saintenoy et al.,
153 2013). At the adjacent polythermal Midtre Lovénbreen, previous research has
154 highlighted up-glacier migration of the boundary between cold- and warm-
155 based ice that was identified from GPR surveys undertaken in 1998 and 2006
156 (Rippin et al., 2007). Evolution of the thermal regime in response to climatic
157 warming and thinning of the ice is also recognised at other Svalbard glaciers
158 (e.g. Hodgkins et al., 1999).

159 In common with other glaciers in the area, the glacier terminus of Austre
160 Lovénbreen has receded by around 1 km since the Neoglacial maximum extent

161 at the end of the nineteenth century. The adjacent Midtre and Vestre
162 Lovénbreen were photographed by Hamberg (1894) in 1892 with high, near-
163 vertical ice margins, at what is now probably the outer part of the moraine-
164 mound complex surrounding each glacier. Given that Austre Lovénbreen is
165 comparable to these glaciers in most respects, it seems likely that it exhibited
166 similar features and reached its Neoglacial maximum at around the same time.
167 The photographic evidence of the Lovénbreen glaciers also corresponds with
168 the work by Svendsen and Mangerud (1997) on the response of Linnébreen in
169 central Spitsbergen indicating Neoglacial distal moraine formation during the
170 late nineteenth century. Overridden soil and vegetation, now found beneath
171 the nearby Longyearbreen, indicate that c. 1100 years ago the margin of the
172 glacier was at least 2 km upstream of the current margin (Humlum et al.,
173 2005). As this glacier is typical of central Spitsbergen glaciers in terms of
174 topographic setting, aspect and size (Humlum et al., 2005), it seems likely that
175 Austre Lovénbreen has experienced a similar advance and recession to that of
176 Longyearbreen over a timescale of over 1100 years.

177 The continuing terminus recession of Austre Lovénbreen is associated with the
178 typically negative mass balance of the glacier that is demonstrated by the
179 mass balance record from 1968 to 2009 at the adjacent Midtre Lovénbreen
180 (WGMS, 2011). Friedt et al. (2012) show the Austre Lovénbreen glacier front
181 positions mapped in 1962, 1995 and 2009. Between 1962 and 1995 the glacier
182 receded by ~300 m, and between 1995 and 2009 the glacier receded by
183 ~75 m.

184 The moraine complex in front of Austre Lovénbreen consists of well-developed
185 high-relief (c. 30–60 m high) lateral moraines, completely detached from the
186 glacier, which continue and merge into the frontal outer moraine complex (c.
187 10 m high) with a distinct difference in morphology to the low-relief
188 (commonly around 5 m high) ‘hummocky moraine’ areas within the moraine-
189 mound complex (Fig. 2).

190 The west coast of Spitsbergen experiences a much warmer climate than its
191 79°N location might imply, with Ny-Ålesund having a mean annual
192 temperature of -6.3 °C from 1961 to 1990 and -5.2 °C from 1981 to 2010
193 (Førland et al., 2011).

194

195 **4. Methods**

196 A pulseEKKO Pro ground-penetrating radar (GPR) system was used with a
197 400 V transmitter and 100 MHz centre frequency antennae to investigate the
198 subsurface characteristics along a series of transects over the outer lateral-
199 frontal moraine complex of Austre Lovénbreen (see Fig. 2B for transect
200 locations). The fieldwork was undertaken during winter conditions in April 2012
201 to ensure the presence of frozen ground. The moraines were covered with a
202 surface ice layer (where this ice layer was visible, it was typically ~5 cm thick)
203 and overlying snow. Whilst snow depth was spatially variable, based upon 45
204 measurements taken at fixed interval along the transects, snow depth was
205 generally less than 5 cm, but was exceptionally as deep as 88 cm. Whilst the
206 majority of the outer moraine had limited snow cover, it was not possible to

207 survey complete transects through and beyond the moraine limits. This was
208 because the prevailing wind through Kongsfjorden at the time the research
209 was undertaken had resulted in deep snow and the formation of large cornices
210 on the NW side of the moraines, which combined with the steep slope of the
211 ice-distal outer moraine face, made both topographic and radar surveys
212 impossible to complete on the ice-distal faces. The 100 MHz antennae were
213 used with the standard 1 m separation and a 0.25 m step size along each
214 transect. A 750 ns time window was used, along with 36 stacks and each trace
215 was manually triggered with the transmitter and receiver stationary and
216 positioned along a 100 m tape. A perpendicular broadside antennae
217 configuration was used with each transect transverse to the moraine ridge
218 crest orientation. The GPR control unit was positioned at least 5 m away from
219 the transmitter and receiver to mitigate any potential signal interference.
220 Velocity was calibrated along each transect with common mid-point (CMP)
221 surveys orientated perpendicular to the main transect (and parallel to the
222 moraine crest). Because the field interpretation of the main reflection-mode
223 transects was that of dipping reflectors, reflection surveys were also
224 undertaken along the line of the CMP surveys to ensure that the CMP survey
225 lines were, as far as possible, parallel to the strike and normal to the direction
226 of dip of the reflectors. The separation distance of the antennae that was
227 completed on each CMP survey was dependent upon the substrate conditions,
228 and ranged from 26–40 m separation, with 40 m being the limit of the fibre
229 optic cable length. An automatic level was used to survey height change along
230 each transect so that the topography could be applied to the radar profiles.

231 Radar profiles were produced using the EKKO_View Deluxe software from
232 Sensors and Software. Dewow, an automatic gain control and topography were
233 applied to each data set during post-processing. A total of 9 reflection-mode
234 main surveys and an additional 17 CMP-mode surveys were obtained around
235 the Austre Lovénbreen lateral-frontal complex.

236 Structural mapping of the glacier surface was undertaken from two images.
237 The first is a monochrome oblique aerial image from 1936 obtained by Norsk
238 Polarinstitut. The second image is an orthorectified aerial image of the lower
239 ~2 km of the glacier tongue and its proglacial area obtained by the NERC ARSF
240 (Natural Environment Research Council, Airborne Research and Survey Facility)
241 in 2003. The 2003 image was derived from 8 scanned true colour contact
242 prints with a resulting spatial resolution of around 1 m.

243

244 **5. Results**

245 *5.1. CMP surveys*

246 The CMP surveys that cross transects 1–5 show ground velocity characteristics
247 that range from 0.16–0.17 m ns⁻¹ (Table 1). CMP surveys that cross transects
248 6–7 have a velocity of 0.15 m ns⁻¹, whereas CMP surveys that cross transects
249 8–9 show ground velocity characteristics that range from 0.13–0.14 m ns⁻¹
250 (Table 1). As an example, Fig. 3a shows a CMP survey across transect 2 with
251 an initial air wave of 0.3 m ns⁻¹, a ground wave around 0.22 m ns⁻¹ through
252 the snow and a subsurface velocity of 0.17 m ns⁻¹. In contrast, Fig. 3b shows a

253 CMP survey across transect 9 with an initial air wave and a subsurface velocity
254 of 0.13 m ns^{-1} .

255

256 *5.2. Internal structure of the moraine*

257 Multiple up-glacier dipping reflectors that intersect both the ice-proximal and
258 ice-distal faces of the moraine are found in all transects (Figs. 4 and 5). These
259 reflectors are common in transect 1, abundant in transects 2–6 and isolated
260 examples occur in transects 7–9 (Figs. 4 and 5 and Table 2). The reflectors
261 often have an asymptotic profile where the dip become progressively shallower
262 at depth; a characteristic that is shown with particular clarity in transect 2
263 (Figs. 4 and 5). The apparent angle of dip of the reflectors at the intersection
264 of the ground surface ranges from $6\text{--}50^\circ$ (Table 3). The reflector apparent dip
265 angles appear reasonably consistent through transects 2–6, with a dominant
266 $41\text{--}50^\circ$ range. However, transect 1 shows lower apparent dip angles with an
267 $11\text{--}20^\circ$ dominant range. Transects 7 and 9 are distinct from the other profiles
268 with lower dip angles dominantly within the $20\text{--}39^\circ$ range, but also including
269 examples below 10° , and transect 8 has a dominant range of $31\text{--}40^\circ$. Transect
270 6 very clearly demonstrates an open syncline structure of reflectors dipping
271 up-glacier in the distal part of the moraine and dipping down-glacier in the
272 proximal part of the moraine (Figs. 4 and 5). This syncline structure is also
273 found in transects 1, 3–4 and 5, but is shown in these examples with less
274 clarity than in transect 6. Transects 7–9 show a number of surface parallel
275 reflectors below the air and surface wave of the GPR profiles (Figs. 4 and 5).

276

277 5.3. *Hyperbolae from point targets*

278 A hyperbolic curve developed over sequential radar traces is created by a point
279 target. Hyperbolae are rare in transects 2–5, in contrast to transects 1 and 6
280 that show a greater number of hyperbolae (Table 2). The dipping reflectors in
281 transects 1 and 6 are, to an extent, slightly obscured by these numerous point
282 hyperbolae. The GPR transects did not have a migration process applied
283 because the dipping tails of each hyperbola can be clearly differentiated from
284 the dipping reflectors. Transects 7–9 reveal a markedly different radar facies
285 that are characterised by multiple overlapping hyperbolae and a lack of clearly
286 identifiable reflectors, in contrast to the surveys along transects 1–6.

287

288 5.4. *Signal attenuation*

289 Transects 1–5 each show clearly identifiable reflector layers down to 15 m
290 depth and in some places down to 20 m depth associated with low signal
291 attenuation (Table 2). Penetration in transect 6 is slightly reduced at 10–15 m
292 depth, but transects 7–9 are markedly different with a lack of clarity below 5 m
293 and an absence of clarity below 10 m depth associated with high signal
294 attenuation (Table 2).

295

296 5.5 *Glacier structural mapping*

297 An assessment of the structural composition of Austre Lovénbreen in 1936 has
298 been undertaken using oblique aerial imagery (Fig. 6). The lowermost ~1 km

299 of the terminus is mapped in greater detail since it is nearer to the viewer and
300 hence the structures more readily identified. In 1936 the glacier had barely
301 receded from its Neoglacial maximum position, although the flat terminus
302 where the glacier met the moraine indicates that it had experienced thinning at
303 the terminus. This is in contrast to the steep terminal ice cliffs described by
304 Hamberg (1894) when the area was visited in 1892.

305 A number of structural features are identified (Fig. 6). Primary stratification is
306 produced originally by snow accumulation in horizontal layers and is found: (1)
307 within one flow unit of the glacier that has been deformed into a nested set of
308 arcuate bands; and (2) as bands stretching across much of the frontal margin,
309 although best developed on the true left of the glacier (Fig. 6).

310 The longitudinal features stretching up-glacier from the ice margin are
311 interpreted as longitudinal foliation. This structure appears around much of the
312 glacier margin, although there are clear concentrations of longitudinal foliation
313 which appear to have released significant quantities of sediment onto the
314 glacier surface.

315 There are also isolated debris-laden fractures in the upper true left terminus.
316 The precise origin of these features is uncertain, but they could represent
317 debris-filled crevasse traces, debris-rich primary stratification, or englacial
318 thrust faults laden with basal sediment.

319 One intriguing feature of the 1936 imagery is a bulge in the glacier surface
320 from the true left valley side across around two thirds of the glacier width
321 (indicated by the thick dotted line on Fig. 6). This bulge is best identified by

322 tracing the prominent longitudinal foliation up-glacier and the slope of the true
323 left lateral margin. The origin and significance of this bulge is uncertain, but it
324 would be consistent with a surge wave propagating down-glacier in 1936.

325 The quality of the 2003 aerial imagery allows a much more detailed structural
326 assessment of Austre Lovénbreen to be mapped (Fig. 7). Three primary flow
327 units are identified, defined by dense areas of longitudinal foliation that can be
328 traced as far up-glacier as the imagery presented permits. These may
329 represent medial moraines produced at the confluence of individual flow units.

330 Primary stratification is a prominent feature in the 2003 imagery and is
331 seemingly more extensive than is shown in the 1936 image. Much of the
332 primary stratification is folded, indicating lateral compression, and where it can
333 be picked out along the trace of longitudinal foliation, is shown to be tightly
334 folded with the fold limbs extending along the axis of flow. Primary
335 stratification is generally less folded in the true left flow unit.

336 Longitudinal foliation is a ubiquitous feature around the glacier margin where it
337 releases significant quantities of sediment. Many of the foliae melting out on
338 the glacier surface can be traced linearly into the proglacial zone. Although
339 longitudinal foliation is concentrated along medial moraine features at flow unit
340 boundaries (cf. Hambrey and Glasser, 2003), this structure can be traced up-
341 glacier from almost any point from the ice margin. There are significant
342 concentrations of longitudinal foliation along the lateral margins, and through
343 much of the central flow unit.

344 Debris-bearing fractures are mapped close to the true right margin. It is
345 unclear what the origin of these features could be, as was the case for the
346 1936 imagery, and we advance the same hypotheses for their origin. Notably,
347 these features do not appear in the same location as in the 1936 imagery.

348 The higher resolution 2003 image allows the mapping of more subtle features
349 including crevasses and crevasse traces. Open crevasses are generally rare,
350 and most such features mapped are in fact crevasse traces (Fig. 7). The
351 highest density of crevasse traces can be found along the true left flow unit.
352 Crevasse traces are also found along the true right lateral margin, but the
353 density of crevasse-related features here is much lower. Crevasse traces along
354 the true right are relatively short (~150 m in length) compared with the
355 extensive (up to ~500 m long) arcuate crevasse traces across the centre of the
356 glacier terminus.

357

358 **6. Discussion**

359 *6.1. Moraine composition*

360 The CMP surveys revealed radar velocities through the moraine of between
361 0.13 and 0.17 m ns⁻¹, indicating that its composition is varied. High velocities
362 (at, or close to the 0.17 m ns⁻¹ velocity through glacier ice; Murray and Booth,
363 2010; Saintenoy et al., 2013), combined with low signal attenuation and
364 associated deep penetration, are characteristic of a large ice component (Table
365 4). Lower velocities and relatively higher signal attenuation are indicative of a
366 significant sediment component. Schwamborn et al. (2008) determined the

367 radar velocity through unsorted 'outwash [and] morainic deposits' in the
368 proglacial area of the adjacent Midtre Lovénbreen to be 0.127 m ns^{-1} . The
369 sequence at Midtre Lovénbreen, which appears to be mostly clast-rich
370 intermediate diamicton (Fig. 8 in Schwamborn et al., 2008), was just under
371 3 m thick with a mean ice content of around 10% (gravimetric ice content
372 expressed as water equivalent, as determined from a 6 cm diameter
373 permafrost core) and is a common facies in the proglacial setting of Midtre
374 Lovénbreen (Midgley et al., 2007). Although frozen ground conditions
375 prevented us from directly determining the nature of the sediments within the
376 Austre Lovénbreen lateral moraine, previous work has found clast-rich
377 diamicton to be abundant within this moraine-mound complex (Graham, 2002).
378 Given the consistent geology underlying the two glaciers and the proximity of
379 the sites, it is likely that velocities of around 0.13 m ns^{-1} are indicative of
380 frozen diamicton with around 10% interstitial ice at Austre Lovénbreen. Based
381 upon the known radar velocity through both glacier ice (0.17 m ns^{-1}) consisting
382 of ~100% ice and a known velocity for a proglacial debris facies with ~10%
383 interstitial ice component (0.127 m ns^{-1}), a linear interpolation between these
384 two end members can be used to estimate likely velocities for a range of
385 debris-ice mixes (Table 5).

386 The observed radar velocities of 0.16 to 0.17 m ns^{-1} across transects 1 to 5 are
387 characteristic of a dominant ice component within the outer moraine complex
388 with up to 20% sediment. Radar velocities along transects 6 and 7 still indicate
389 a significant ice component, but with up to 40% sediment. Radar velocities

390 along transects 8 and 9 are indicative of a relatively low ice component, with
391 sediment contributing between 60% and 80% of the moraine volume.

392

393 *6.2. Identification of debris within the substrate*

394 Four distinct zones (A–D) of the lateral-frontal outer moraine complex at
395 Austre Lovénbreen are recognised (Fig. 2) on the basis of both the ice-debris
396 mix and the structural characteristics.

397 Zone A, whilst having a dominant ice component, does exhibit hyperbolae,
398 which are likely to indicate the presence of isolated coarse-grained clastic
399 material within the ice (Fig. 4). This is in contrast to zone B, which also has a
400 dominant ice component, but appears to lack the isolated coarse-grained
401 component that would cause hyperbolae in the radar profiles (Fig. 4). The
402 measured velocity in zone C of transect 6 is the same as that of transect 7, but
403 a high coarse-grained debris load is inferred for transect 7 that inhibits the
404 identification of any structural features (Fig. 4). This is in contrast to the fine-
405 grained debris load found in transect 6, which results in identification of the
406 clear structural characteristics. Zone D has a dominant coarse-grained debris
407 component shown by the ubiquitous overlapping hyperbolae (Fig. 4).

408

409 *6.3. Structural glaciology and dynamics of Austre Lovénbreen*

410 The structural mapping of Austre Lovénbreen provides important context that
411 aids the understanding of the conditions under which the lateral-frontal
412 moraine formed. A number of features indicate that the glacier is now far less

413 dynamic than it would have been during its Neoglacial maximum extent. Most
414 notably, there were few actively forming crevasses in 2003 (Fig. 7), indicating
415 that the glacier is now flowing very slowly. The 1936 imagery (Fig. 6) is not of
416 sufficient resolution to identify crevasses, but there is evidence that Austre
417 Lovénbreen had a surface bulge. Further analysis is required in order to
418 determine whether this was a surge-related expression, but the dense
419 population of fractures (interpreted here mostly as crevasse traces) along the
420 true left side of the glacier, close to the ice margin, indicates that this flow unit
421 was more dynamic in the past.

422 If there had been a surge around 1936, it will not have contributed ice to the
423 ice-core within the lateral-frontal moraines that are under investigation here. It
424 is possible, however, that a surge may have allowed pushing of the glacier
425 against the lateral-frontal moraine and thereby allowed some deformation of
426 the ice-core. Another possibility is that the glacier surged during its Neoglacial
427 advance and that the ice preserved in the lateral-frontal moraine is derived
428 from such a surge. Hansen (2003) suggested that neighbouring Midtre
429 Lovénbreen had once been a surge-type glacier, but could no longer be
430 considered to be so. We suggest, albeit tentatively, that Austre Lovénbreen
431 may once have been a surge-type glacier, but there is no indication that it has
432 surged since ~1936, nor is there any indication that it will surge again in the
433 near future.

434

435 *6.4. Origin of ice incorporated within the lateral-frontal moraine*

436 The structural maps of Austre Lovénbreen provide important context that aid
437 understanding of the origin of the ice now found within the lateral-frontal
438 moraine. The GPR surveys demonstrate that the ice within the moraine
439 contains a combination of ice and debris arranged in layers, some of which
440 have experienced folding.

441 The up-glacier dipping reflectors with minor folding (Fig. 5) are consistent with
442 the structural characteristics of layered primary stratification, as seen in the
443 1936 oblique aerial image (Fig. 6). Hambrey et al. (2005), for example,
444 showed in a longitudinal GPR profile (i.e. orientated parallel with ice flow) that
445 primary stratification at neighbouring Midtre Lovénbreen dipped up-glacier,
446 and had experienced minor folding. However, primary stratification is not likely
447 to contain the significant quantities of debris revealed by the GPR survey. The
448 layering of primary stratification instead usually results from differences in
449 crystallography and bubble content.

450 Debris-bearing structures exist in the terminus of Austre Lovénbreen that are
451 transverse to flow (Figs. 6 and 7). These structures could represent isolated
452 englacial thrusts. It would, however, also be hard to envisage that these
453 isolated features could explain the dense layering shown in the GPR surveys of
454 the moraine. It could be argued, however, that our mapping, without any
455 ground-truthing of the structures, may have under-represented the number of
456 debris-bearing fractures, including thrusts. In particular, there are numerous
457 arcuate fractures that extend across much of the lower part of the terminus,
458 some of which may include thrusts. Indeed, Hambrey et al. (2005) interpreted
459 similar arcuate fractures at Midtre Lovénbreen as englacial thrust planes.
460 Nonetheless, it is hard to envisage that all of the reflectors in the GPR profiles

461 represent englacial thrusts. Other studies have identified debris-rich englacial
462 thrusts with GPR at a number of other glaciers in the region, including Scott
463 Turnerbeen (Sletten et al., 2001), Bakaninbreen (Murray et al., 1997) and
464 nearby Kongsvegen (Murray and Booth, 2010). Radar images of dipping
465 reflectors from Austre Lovénbreen appear distinct from englacial thrust
466 reflectors reported at Kongsvegen by Murray and Booth (2010) which, at
467 Kongsvegen, appear to be isolated, discrete and thicker features than are
468 found at Austre Lovénbreen.

469 A further possibility is that the dipping structures within the moraine represent
470 layering within buried basal ice. Debris-laden basal ice commonly has a layered
471 appearance derived either from freeze-on of packages of water and sediment
472 to the glacier base, or from regelation, and may have a sediment content from
473 0 to ~90% (e.g. Hubbard and Sharp, 1989; Knight, 1997; Hubbard et al.,
474 2009). Further, the folding in the layers is also consistent with reports of
475 tectonic deformation within basal ice layers (e.g. Waller et al., 2000), perhaps
476 in this case caused by compression against the adverse bed slope, or the cold-
477 based margin, or possibly during a surge event. Several processes could
478 contribute to basal ice formation at Austre Lovénbreen including regelation as
479 the glacier slides over bedrock in the temperate zone up-glacier from the
480 terminus (e.g. Hubbard and Sharp, 1993), and seasonal freeze-on of
481 meltwater and sediment at the glacier terminus (e.g. Weertman, 1961).
482 Additionally, analysis of the GPR profile of Saintenoy et al. (2013)
483 demonstrates that the adverse bed slope of the basin beneath Austre
484 Lovénbreen is ~1.6 times steeper than the ice surface slope. Hence, the bed
485 slope meets the threshold necessary to permit the operation of glaciohydraulic

486 supercooling and associated freeze-on of water and sediment (e.g. Lawson et
487 al., 1998; Cook et al., 2010). There are no reports, however, of any field
488 evidence diagnostic of the operation of supercooling (cf. Evenson et al., 1999;
489 Cook et al., 2006). Regelation is unlikely to produce the thick sequences of ice
490 and sediment shown in the GPR profiles, as basal ice thicknesses associated
491 with regelation are generally less than ~1m due to ice melting from the base
492 during glacier sliding (e.g. Hubbard and Sharp, 1989; Knight, 1997). Basal ice
493 could be formed by freeze-on, either seasonally or possibly through
494 supercooling. Our favoured hypothesis is that post-formational flow-related
495 deformation in the form of strong longitudinal compression has led to the
496 stacking of the debris-rich layers (e.g. Waller et al., 2000). Strong longitudinal
497 compression could be caused by either: (1) the subglacial overdeepening
498 (based on our interpretation of the GPR profiles undertaken by Saintenoy et al.,
499 2013); (2) the glacier margin during the Neoglacial maximum; or (3)
500 associated with a surge.

501 The buried basal ice could be composed of a range of descriptively different
502 facies, possibly with different origins. However, at the resolution of the radar
503 imagery the most appropriate classification is banded basal ice (i.e. layering on
504 the scale of centimetres to decimetres), according to the classification scheme
505 of Hubbard et al. (2009). Care must be taken with the interpretation of the
506 reflector angle of dip as the survey lines may not run parallel to the direction
507 of dip of the reflectors in each case. What is recorded, therefore, is an
508 apparent dip, rather than an actual dip. Further work involving three-
509 dimensional GPR profiling of the reflectors could resolve this issue.

510

511 6.5. *Landform stability and preservation potential*

512 Despite its high ice content, the moraine within zones A–C appears relatively
513 stable. Examination of aerial imagery reveals an absence of slope failure and
514 back wasting features (Fig. 2) that are characteristic of moraines with high
515 rates of ablation of incorporated buried ice (e.g. Bennett et al., 2000). It is,
516 however, likely that surface lowering is occurring, as repeat lidar surveys of
517 the north east side of the outer complex at the adjacent Midtre Lovénbreen has
518 shown surface lowering of 0.65 m a^{-1} ($\pm 0.2 \text{ m}$) (Irvine-Fynn et al., 2011).
519 Schomaker and Kjær (2008) also recognised similar downwasting rates of
520 0.9 m a^{-1} from 1983 to 2004 at Holmströmbreen in central Spitsbergen. Given
521 the mean summer temperature of $3.8 \text{ }^\circ\text{C}$ recorded during the 1981-2010
522 period at nearby Ny-Ålesund (Førland et al., 2011), it is likely that the buried
523 ice at Austre Lovénbreen experiences some ablation during the summer
524 months. So zones A–C of the outer moraine complex are downwasting, rather
525 than backwasting. The dampening effect on ablation of the thin protective
526 surface debris layer will depend upon: (1) the thickness of the debris layer; (2)
527 the thermal conductivity of the debris type; and (3) the water content of the
528 surface debris layer (Schomacker, 2008). Other potential factors that result in
529 a difference between the stability of the surface debris layer of the ice-cored
530 lateral moraines at Austre Lovénbreen and nearby Kongsvegen (outlined by
531 Bennett et al., 2000) include a potentially thicker surface debris layer and/or
532 coarser surface debris that promote drainage. A freely drained surface debris
533 layer would be less prone to slope failure and exposure of the underlying ice,
534 but would have a higher thermal conductivity, so could act to either promote

535 or inhibit the ablation of the buried ice. Rates of dead-ice ablation can be
536 similar in both the cold arid Svalbard climate and the mild humid climate of
537 Iceland (Schomaker and Kjær, 2008). This outer moraine complex at Austre
538 Lovénbreen is located away from the proglacial fluvial discharge routes of both
539 Austre and Midtre Lovénbreen: this is likely to be the key issue facilitating the
540 lack of backwasting and apparent stability of the landform.

541 The moraine within zone D contains a relatively small amount of ice and the
542 porosity of the debris is, therefore, important to understand how the
543 incorporated ice influences its morphology. Whilst Kilfeather and van der Meer
544 (2008) note that 'till porosity has largely been ignored', a range of likely
545 porosity values can be assessed (Table 6). The Austre Lovénbreen outer
546 moraine is likely to have a porosity value of between 0.15 and 0.30, based
547 upon comparison to other similar sedimentary and morphological settings. The
548 outer moraine within zone D at Austre Lovénbreen is, therefore, likely to
549 experience little modification associated with the removal of 20–40%
550 interstitial ice. High preservation potential of the outer moraine morphology in
551 zone D is, therefore, likely to occur even following the complete ablation of the
552 incorporated ice.

553

554 **7. Conclusions**

555 1. Buried ice forms the dominant component of the Austre Lovénbreen
556 outer moraine in the upper lateral zone, whereas sediment forms the
557 dominant component of the frontal zone.

- 558 2. Many examples of ice forming unstable components of landforms have
559 been recognised and are associated with sediment reworking, but this
560 example at Austre Lovénbreen illustrates that ice can, so far, form a
561 relatively stable component of landforms without sediment reworking,
562 although landform degradation will still occur.
- 563 3. The rate of surface lowering associated with ablation of buried ice is
564 likely to have increased associated with the local change from a summer
565 temperature of 3.4 °C (1961–1990) to 3.8 °C (1981–2010). This
566 ablation rate is likely to increase further if local air temperature also
567 increases.
- 568 4. Because of the ice-debris mix within the outer moraine, following
569 complete climatic amelioration, the preservation potential of any
570 geomorphological feature associated with the upper lateral moraine
571 (zones A–B) is negligible. The preservation potential of the frontal
572 moraine, however, is high, with little change predicted in the
573 contemporary geomorphology resulting from the complete meltout of the
574 interstitial ice component that is currently preserved by the low
575 temperature and lack of ice exposure by surface sediment reworking.
- 576 5. The ice within the lateral-frontal moraine is likely to be composed of
577 basal ice derived from freeze-on of ice and sediment to the glacier bed.
578 Post-formational deformation, in the form of strong longitudinal
579 compression, has subsequently led to a stacking and thickening of the
580 sequence.
- 581 6. The glacier surface bulge identified on the 1936 aerial imagery provides
582 evidence that Austre Lovénbreen has previously displayed surge activity,

583 although given the current state of the thermal regime and recent mass
584 balance it is highly unlikely to do so in the near future.

585 7. This research shows the value of relict buried ice that is preserved in
586 landforms to aiding our understanding of former glacier characteristics.

587 8. Further research on the stable isotope composition, sedimentology of
588 included debris, and crystallography of the buried ice at Austre
589 Lovénbreen will aid our understanding of both its origin and its value as
590 an archive of palaeoglaciological information from the Neoglacial.

591

592 **Acknowledgements**

593 The research was funded by grants from Nottingham Trent University (to NGM)
594 and the Royal Society (2007/R2 to DJG/NGM). The fieldwork benefited from
595 the logistical support provided by Steinar Aksnes of the Norwegian Polar
596 Institute's Sverdrup Station. Tris Irvine-Fynn is thanked for the provision of
597 height data for a number of positions outside of the moraine-mound complex.
598 This manuscript benefitted from reviews and editorial comment by three
599 anonymous reviewers and Richard Marston.

600

601 **References**

- 602 Bennett, M.R., Huddart, D., Glasser, N.F., Hambrey, M.J., 2000.
603 Resedimentation of debris on an ice-cored lateral moraine in the high-Arctic
604 (Kongsvegen, Svalbard). *Geomorphology* 35 (1–2), 21–40.
- 605 Boulton, G.S., Eyles, N., 1979. Sedimentation by valley glaciers: a model and
606 genetic classification. In: Schluchter, C. (Ed.), *Moraines and Varves*. Balkema,
607 Rotterdam, pp. 11–23.
- 608 Burki, V., Hansen, L., Fredin, O., Andersen, T.A., Beylich, A.A., Jaboyedoff, M.,
609 Larsen, E., Tønnesen, J.-F. 2010. Little Ice Age advance and retreat sediment
610 budgets for an outlet glacier in western Norway. *Boreas* 39 (3), 551–566.
- 611 Cook, S.J., Waller, R.I., Knight, P.G., 2006. Glaciohydraulic supercooling: the
612 process and its significance. *Progress in Physical Geography* 30 (5), 577–588.
- 613 Cook S.J., Robinson Z.P., Fairchild, I.J., Knight, P.G., Waller, R.I., Boomer, I.,
614 2010. Role of glaciohydraulic supercooling in the formation of stratified facies
615 basal ice: Svínafellsjökull and Skaftafellsjökull, southeast Iceland. *Boreas* 39
616 (1), 24–38.
- 617 Cook, S.J., Graham, D.J., Swift, D.A., Midgley, N.G., Adam, W.G., 2011.
618 Sedimentary signatures of basal ice formation and their preservation within
619 ice-marginal sediments. *Geomorphology* 125 (1), 122–131.
- 620 Embleton, C., King, C.A., 1975. *Glacial and Periglacial Geomorphology*, Arnold,
621 London.

622 Etzelmüller, B., Ødegård, R.S., Vatne, G., Mysterud, R.S., Tønning, T., Sollid,
623 J.L., 2000. Glacier characteristics and sediment transfer system of
624 Longyearbreen and Larsbreen, western Spitsbergen. *Norsk Geografisk*
625 *Tidsskrift* 54 (4), 157–168.

626 Evans, D.J.A., 2009. Controlled moraines: origins, characteristics and
627 palaeoglaciological implications. *Quaternary Science Reviews* 28 (3–4), 183–
628 208.

629 Evenson, E.B., Lawson, D.E., Strasser, J.C., Larson, G.J., Alley, R.B.,
630 Ensminger, S.L., Stevenson, W.E., 1999. Field evidence for the recognition of
631 glaciohydraulic supercooling. In: Mickelson, D.M., Attig, J.W. (Eds.), *Glacial*
632 *Processes: Past and Present*. Geological Society of America, Special Paper 337,
633 pp. 23–35.

634 Ewertowski M., Kasprzak L., Szuman I., Tomczyk A.M., 2012. Controlled, ice-
635 cored moraines: sediments and geomorphology. An example from
636 Ragnarbreen, Svalbard. *Zeitschrift für Geomorphologie* 51 (1), 53–74.

637 Flint, R.F., 1971. *Glacial and Quaternary geology*. John Wiley and Sons, New
638 York.

639 Førland, E.J., Benestad, R., Hanssen-Bauer, I., Haugen, J.E., Skaugen, T.E.,
640 2011. Temperature and precipitation development at Svalbard 1900–2100.
641 *Advances in Meteorology*, 893790.

642 Friedt, J-M., Tolle, F., Bernard, É., Griselin, M., Laffly, D., Marlin, C., 2012.
643 Assessing the relevance of digital elevation models to evaluate glacier mass

644 balance: application to Austre Lovénbreen (Spitsbergen, 79°N). *Polar Record*
645 48 (244), 2–10.

646 Glasser, N.F., Hambrey, M.J., 2003. Ice-marginal terrestrial landsystems:
647 Svalbard polythermal glaciers. In: Evans, D.J.A. (Ed.) *Glacial Landsystems*.
648 Hodder Arnold, London, pp. 65–88.

649 Graham, D.J., 2002. Moraine-mound formation during the Younger Dryas in
650 Britain and the Neoglacial in Svalbard. PhD thesis, University of Wales,
651 Aberystwyth, UK.

652 Hagen, J.O., Leistøl, O., Roland, E., Jørgensen, T., 1993. *Glacier atlas of*
653 *Svalbard and Jan Mayen*. Norsk Polarinstitut, Meddelelser.

654 Hamberg, A., 1984. En resa till norra Ishafvet sommaren 1892. *Ymer* 14, 25–
655 61.

656 Hambrey, M.J., Glasser, N.F., 2003. The role of folding and foliation
657 development in the genesis of medial moraines: examples from Svalbard
658 glaciers. *Journal of Geology* 111 (4), 471–485.

659 Hambrey, M.J., Bennett, M.R., Dowdeswell, J.A., Glasser, N.F., Huddart, D.,
660 1999. Debris entrainment and transfer in polythermal valley glaciers. *Journal*
661 *of Glaciology* 45 (149), 69–86.

662 Hambrey, M.J., Murray, T., Glasser, N.F., Hubbard, A., Hubbard, B., Stuart, G.,
663 Hansen, S., Kohler, J., 2005. Structure and changing dynamics of a
664 polythermal valley glacier on a centennial time-scale: midre Lovénbreen,
665 Svalbard. *Journal of Geophysical Research, Earth Surface* F010006.

666 Hansen, S., 2003. From surge-type to non-surge type glacier behaviour: Midre
667 Lovénbreen, Svalbard. *Annals of Glaciology* 36, 97–102.

668 Hodgkins, R., Hagen, J.O., Hamran, S.-E., 1999. Twentieth-century mass
669 balance and thermal regime change at an Arctic glacier. *Annals of Glaciology*
670 28, 216–220.

671 Hubbard, B., Sharp, M.J., 1989. Basal ice formation and deformation: a review.
672 *Progress in Physical Geography* 13 (4), 529–558.

673 Hubbard, B., Sharp, M.J., 1993. Weertman regelation, multiple refreezing
674 events and the isotopic evolution of the basal ice layer. *Journal of Glaciology*
675 39 (132), 275–291.

676 Hubbard, B., Cook, S., Coulson, H., 2009. Basal ice facies: a review and
677 unifying approach. *Quaternary Science Reviews* 28 (19–20), 1956–1969.

678 Humlum, O., Elberling, B., Hormes, A., Fjordheim, K., Hansen, O.H. and
679 Heinemeier, J., 2005. Late-Holocene glacier growth in Svalbard, documented
680 by subglacial relict vegetation and living soil microbes. *The Holocene* 15 (3),
681 396–407.

682 IPCC, 2007. *Climate Change 2007: The physical science basis. Contribution of*
683 *working group I to the fourth assessment report of the Intergovernmental*
684 *Panel on Climate Change.* Solomon, S., Qin, D., Manning, M., Chen, Z.,
685 Marquis, M., Averyt, K.B., Tignor, M.M.B., Miller, H.L. (Eds.). Cambridge
686 University Press, Cambridge, UK and New York, NY, USA, pp. 996.

687 Irvine-Fynn, T.D.L., Barrand, N.E., Porter, P.R., Hodson, A.J., Murray, T., 2011.
688 Recent High-Arctic glacial sediment redistribution: A process perspective using
689 airborne lidar. *Geomorphology* 125 (1), 27–39.

690 Jiskoot, H., Murray, T., Boyle, P.J., 2000. Controls on the distribution of surge-
691 type glaciers in Svalbard. *Journal of Glaciology* 46 (154), 412–422.

692 Kilfeather, A.A., van der Meer, J.J.M., 2008. Pore size, shape and connectivity
693 in tills and their relationship to deformation processes. *Quaternary Science*
694 *Reviews* 27 (3–4), 250–266.

695 Knight, P.G., 1997. The basal ice layer of glaciers and ice sheets. *Quaternary*
696 *Science Reviews* 16 (9), 975–993.

697 Knight, P.G., Patterson, C.J., Waller, R.I., Jones, A.P., Robinson, Z.P., 2000.
698 Preservation of basal-ice sediment texture in ice sheet moraines. *Quaternary*
699 *Science Reviews* 19 (13), 1255–1258.

700 Lawson, D.E., 1979. Sedimentological analysis of the western terminus region
701 of the Matanuska Glacier, Alaska. *Cold Regions Research and Engineering*
702 *Laboratory Report* 79–9, pp. 112.

703 Lawson, D.E., Strasser, J.C., Evenson, E.B., Alley, R.B., Larson, G.J., Arcone,
704 S.A., 1998. Glaciohydraulic supercooling: a freeze-on mechanism to create
705 stratified, debris-rich basal ice: I. Field Evidence. *Journal of Glaciology* 44
706 (148), 547–562.

707 Liestøl, O. 1988. The glaciers in the Kongsfjorden area, Svalbard. *Norsk*
708 *Geografisk Tidsskrift* 42 (4), 231–238.

709 Lønne, I., 2007. Reply to Lukas, S., Nicholson, L.I., Humlum, O. (2006).
710 Comment on Lønne and Lyså (2005): Deglaciation dynamics following the
711 Little Ice Age on Svalbard: Implications for shaping of landscapes at high
712 latitudes. *Geomorphology* 72, 300–319. *Geomorphology*, 86 (1–2), 217–218.

713 Lønne, I., Lauritsen, T., 1996. The architecture of a modern push-moraine at
714 Svalbard as inferred from ground-penetrating radar. *Arctic and Alpine*
715 *Research* 28 (4), 488–495.

716 Lønne, I. and Lyså, A., 2005. Deglaciation dynamics following the Little Ice Age
717 on Svalbard: implications for shaping of landscapes at high latitudes.
718 *Geomorphology* 72 (1–4), 300–319.

719 Lukas, S., Nicholson, L.I., Ross, F.H., Humlum, O., 2005. Formation, meltout
720 processes and landscape alteration of High-Arctic ice-cored moraines –
721 examples from Nordenskiöld Land, Central Spitsbergen. *Polar Geography* 29
722 (3), 157–187.

723 Lukas, S., Nicholson, L.I., Humlum, O., 2007. Comment on Lønne and Lyså
724 (2005): “Deglaciation dynamics following the Little Ice Age on Svalbard:
725 Implications for shaping of landscapes at high latitudes”, *Geomorphology* 72,
726 300–319. *Geomorphology* 84 (1–2), 145–149.

727 Lyså, A., Lønne, I., 2001. Moraine development at a small High-Arctic valley
728 glacier: Rieperbreen, Svalbard. *Journal of Quaternary Science* 16 (6), 519–529.

729 Midgley, N.G., Glasser, N.F., Hambrey, M.J., 2007. Sedimentology, structural
730 characteristics and morphology of a Neoglacial high-Arctic moraine-mound
731 complex: Midre Lovénbreen, Svalbard. In: Hambrey, M.J., Christoffersen, P.,

732 Glasser, N.F., Hubbard, B. (Eds.), *Glacial Sedimentary Processes and Products*,
733 International Association of Sedimentologists, Special Publication 39, pp. 11–23.

734 Murray, T., Booth, A.D., 2010. Imaging glacial sediment inclusions in 3-D using
735 ground-penetrating radar at Kongsvegen, Svalbard. *Journal of Quaternary*
736 *Science* 25 (5), 754–761.

737 Murray, T., Gooch, D.L., Stuart, G.W., 1997. Structures within the surge front
738 at Bakaninbreen, Svalbard, using ground-penetrating radar. *Annals of*
739 *Glaciology* 24, 122–129.

740 Parriaux, A., Nicoud, G.F., 1990. Hydrological behaviour of glacial deposits in
741 mountainous areas. In: Molnár, L. (Ed.), *Hydrology of Mountainous Areas*.
742 International Association of Hydrological Sciences, Publication 190, pp. 291–
743 311.

744 Reynolds, J. 2011. *An Introduction to Applied and Environmental Geophysics*.
745 John Wiley and Sons, Chichester.

746 Rippin, D., Willis, I., Kohler, J., 2007. Changes in the thermal regime of the
747 polythermal Midre Lovénbreen, Svalbard. *Geophysical Research Abstracts* 9,
748 03737.

749 Ronnert, L., Mickelson, D.M., 1992. High porosity of basal till at Burroughs
750 Glacier, southeastern Alaska. *Geology* 20 (9), 849–852.

751 Saintenoy, A., Friedt, J.-M., Booth, A.D., Tolle, F., Bernard, E., Laffly, D.,
752 Marlin C., Griselin, M., 2013. Deriving ice thickness, glacier volume and

753 bedrock morphology of Austre Lovénbreen (Svalbard) using GPR. *Near Surface*
754 *Geophysics* 11 (2), 253–261.

755 Schomacker, A., 2008. What controls dead-ice melting under different climate
756 conditions? A discussion. *Earth-Science Reviews* 90 (3–4), 103–113.

757 Schomaker, A., Kjær, K.H., 2008. Quantification of dead-ice melting in ice-
758 cored moraines at the high-Arctic glacier Holströmbreen, Svalbard. *Boreas* 37
759 (2), 211–225.

760 Schwamborn, G., Heinzl, J., Schirrmeister, L., 2008. Internal characteristics
761 of ice-marginal sediments deduced from georadar profiling and sediment
762 properties (Brøgger Peninsula, Svalbard). *Geomorphology* 95 (1–2), 74–83.

763 Sharp M.J., Jouzel, J., Hubbard, B., Lawson, W., 1994. The character, structure
764 and origin of the basal ice layer of a surge-type glacier. *Journal of Glaciology*
765 40 (135), 327–340.

766 Sletten, K., Lyså, A., Lønne, I., 2001. Formation and disintegration of a high-
767 arctic ice-cored moraine complex, Scott Turnerbreen, Svalbard. *Boreas* 30 (4),
768 272–284.

769 Sugden, D.E., John, B.S., 1976. *Glaciers and Landscape: A Geomorphological*
770 *Approach*. Edward Arnold, London.

771 Swift, D.A., Evans, D.J.A., Fallick, A.E., 2006. Transverse englacial debris-rich
772 ice bands at Kvíárjökull, southeast Iceland. *Quaternary Science Reviews* 25
773 (13–14), 1708–1718.

774 Svendsen, J.-I., Mangerud, J., 1997. Holocene glacial and climatic variations
775 on Spitsbergen, Svalbard. *The Holocene* 7 (1), 45–57.

776 Waller, R.I., Hart, J.K., Knight, P.G., 2000. The influence of tectonic
777 deformation on facies variability in stratified debris-rich basal ice. *Quaternary*
778 *Science Reviews* 19 (8), 775–786.

779 Weertman, J., 1961. Mechanism for the formation of inner moraines found
780 near the edge of cold ice caps and ice sheets. *Journal of Glaciology* 3 (30),
781 965–978.

782 WGMS (2011). *Glacier Mass Balance Bulletin No. 11 (2008–2009)*. Zemp, M.,
783 Nussbaumer, S.U., GärtnerRoer, I., Hoelzle, M., Paul, F., Haeberli, W. (Eds.),
784 ICSU(WDS)/IUGG(IACS)/UNEP/UNESCO/WMO, World Glacier Monitoring
785 Service, Zurich, Switzerland, pp. 102.

786 Worni, R., Stoffel, M., Huggel, C., Volz, C., Casteller, A., Luckman, B., 2012.
787 Analysis and dynamic modeling of a moraine failure and glacier lake outburst
788 flood at Ventisquero Negro, Patagonian Andes (Argentina). *Journal of*
789 *Hydrology* 444–445, 134–145.

790

791 **Table 1** Common mid-point (CMP) survey velocities obtained for each ground-
792 penetrating radar (GPR) transect at Austre Lovénbreen (multiple values
793 indicate velocities obtained from different CMP surveys undertaken along each
794 transect).

Transect	CMP velocity (m ns ⁻¹)
1	0.17
2	0.16 & 0.17
3	0.16
4	0.17
5	0.17, 0.16, 0.16, 0.17 & 0.17
6	0.15 & 0.15
7	0.15
8	0.14
9	0.14, 0.14 & 0.13

795

796 **Table 2** Summary table of radar facies in the Austre Lovénbreen outer lateral-frontal moraine.

Transect	Relative velocity	Signal attenuation	Dipping reflectors	Syncline structure	Surface parallel reflectors	Hyperbolae	Debris component	Ice component	Zone
1	high	low	common	vague	absent	common	limited	dominant	A
2	high	low	abundant	not found	absent	scarce	limited	dominant	B
3	high	low	abundant	vague	absent	scarce	limited	dominant	B
4	high	low	abundant	vague	absent	scarce	limited	dominant	B
5	high	low	abundant	vague	absent	scarce	limited	dominant	B
6	moderate	moderate	abundant	clear	absent	moderate	ice-debris mix	ice-debris mix	C
7	moderate	high	scarce	absent	present	ubiquitous	ice-debris mix	ice-debris mix	C
8	low	high	scarce	absent	present	ubiquitous	dominant	limited	D
9	low	high	scarce	absent	present	ubiquitous	dominant	limited	D

798 **Table 3** Relative abundance of reflector apparent angle of dip at the moraine
 799 surface.

Transect	Apparent angle of dip				
	10°	11-20°	21-30°	31-40°	41-50°
1		•••••	•		
2					•••••
3			•	•	••••
4				•	•••••
5				•	•••••
6			•	••	•••
7	•	••	•••		
8			•	••••	•
9	•	•	•••	•	

800

801

802 **Table 4** Common radar velocities (as cited by Schwamborn et al., 2008;
803 Murray and Booth 2010; Reynolds, 2011).

Material	Radar velocity (m ns ⁻¹)
air	0.3
snow	0.194-0.252
glacier ice	0.168-0.172
permafrost consisting of clast-rich intermediate diamicton with 10% interstitial ice	0.127
water (fresh)	0.033

804

805

806 **Table 5** Known radar velocities and interpreted velocities of ice-debris mixes.

Radar velocity (m ns ⁻¹)	substrate ice component	substrate debris component	interpreted substrate ice component	interpreted substrate debris component
0.17 ^a	100%	0%		
0.16			80%	20%
0.15			60%	40%
0.14			40%	60%
0.13			20%	80%
0.127 ^b	10%	90%		

807 ^a commonly accepted value for glacier ice (e.g. Saintenoy et al., 2013)

808 ^b velocity value for diamicton with 10% interstitial ice found by Schwamborn et
 809 al. (2008) at the adjacent Midtre Lovénbreen

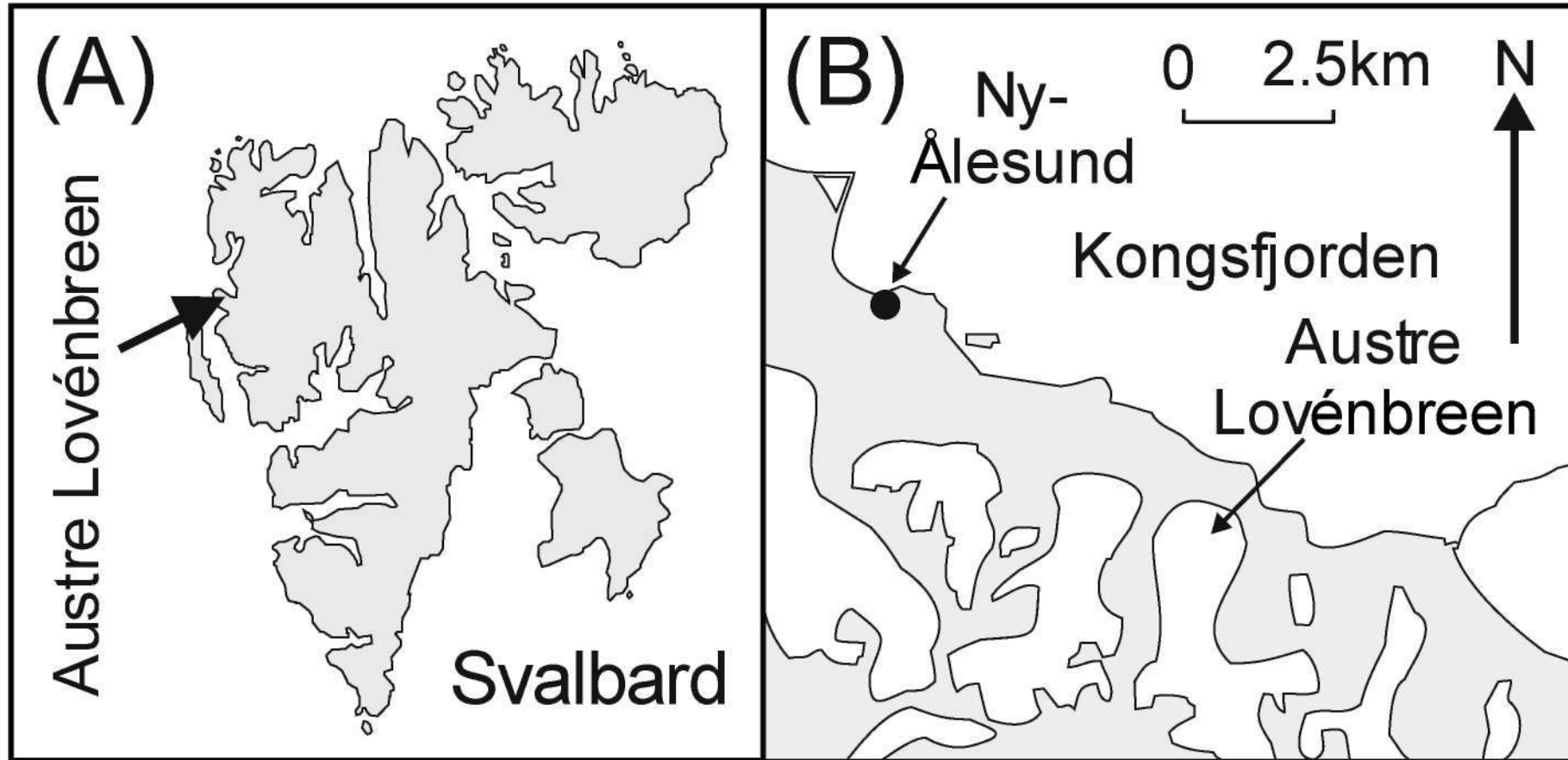
810

811 **Table 6** Example porosities associated with a range of glacial sediments and landforms.

Debris / landform type	Porosity	Source
Pleistocene till samples	0.01-0.19	Kilfeather and van der Meer, 2008
lateral moraine	0.10-0.15	Parriaux and Nicoud, 1990
value used to model terminal moraine failure and associated glacial lake outburst flood	0.15	Worni et al., 2012
frontal moraine	0.15-0.25	Parriaux and Nicoud, 1990
supraglacial till	0.20-0.40	Parriaux and Nicoud, 1990
B0dalen valley diamictos	0.25-0.40	Burki et al., 2010
recently deposited till from debris-rich basal ice	0.26-0.39	Ronnert and Mickelson, 1992
recently deposited diamicton at Matanuska glacier	0.30-0.50	Lawson, 1979

812

813
814
815
816
817
818
819
820
821



822 **Figure 1** Location of: (A) Austre Lovénbreen on Svalbard in the Norwegian high-Arctic; (B) Austre Lovénbreen on
823 Brøggerhalvøya near Ny-Ålesund.

824

825

826

827

828

829

830

831

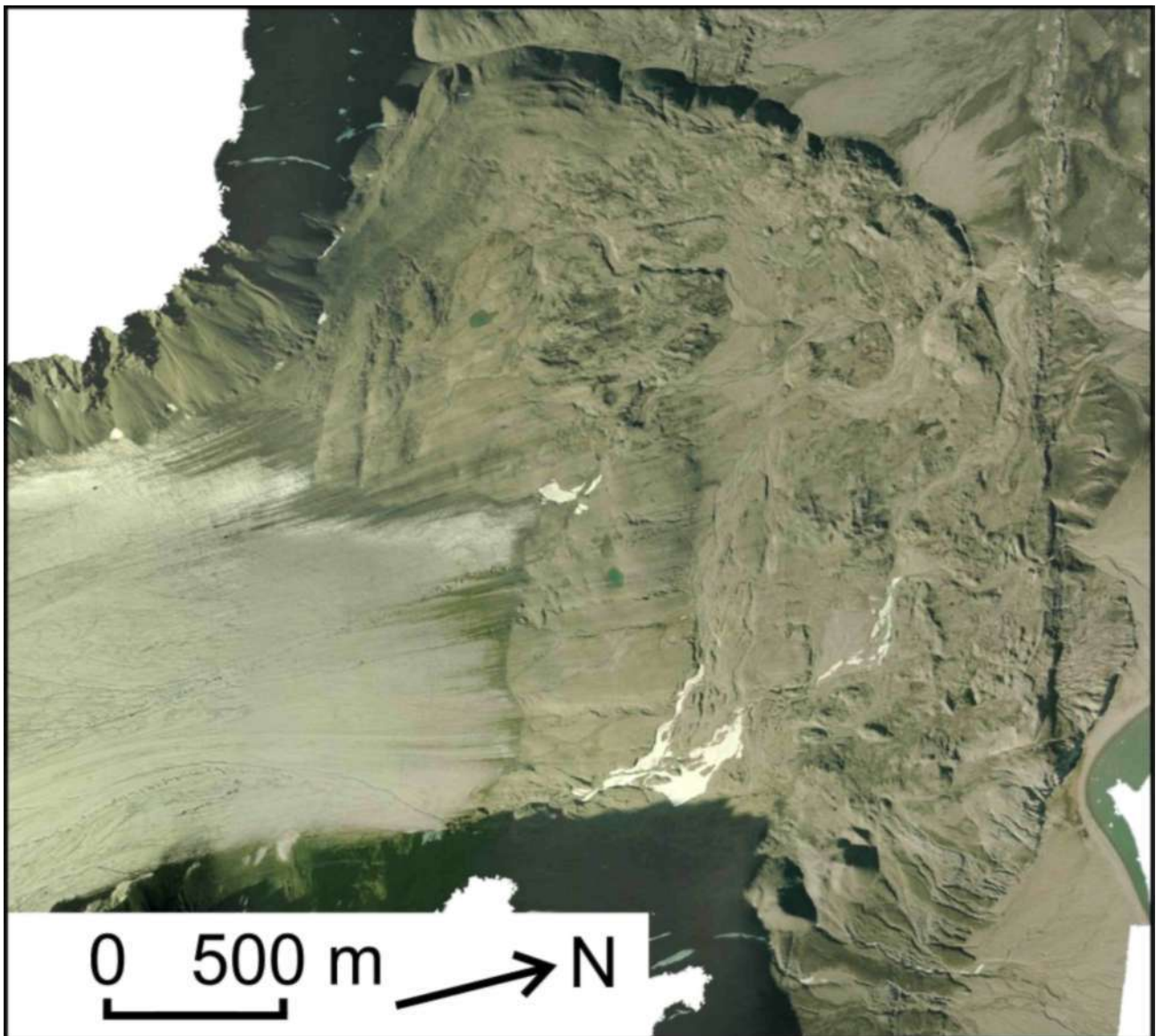
832

833

834

835

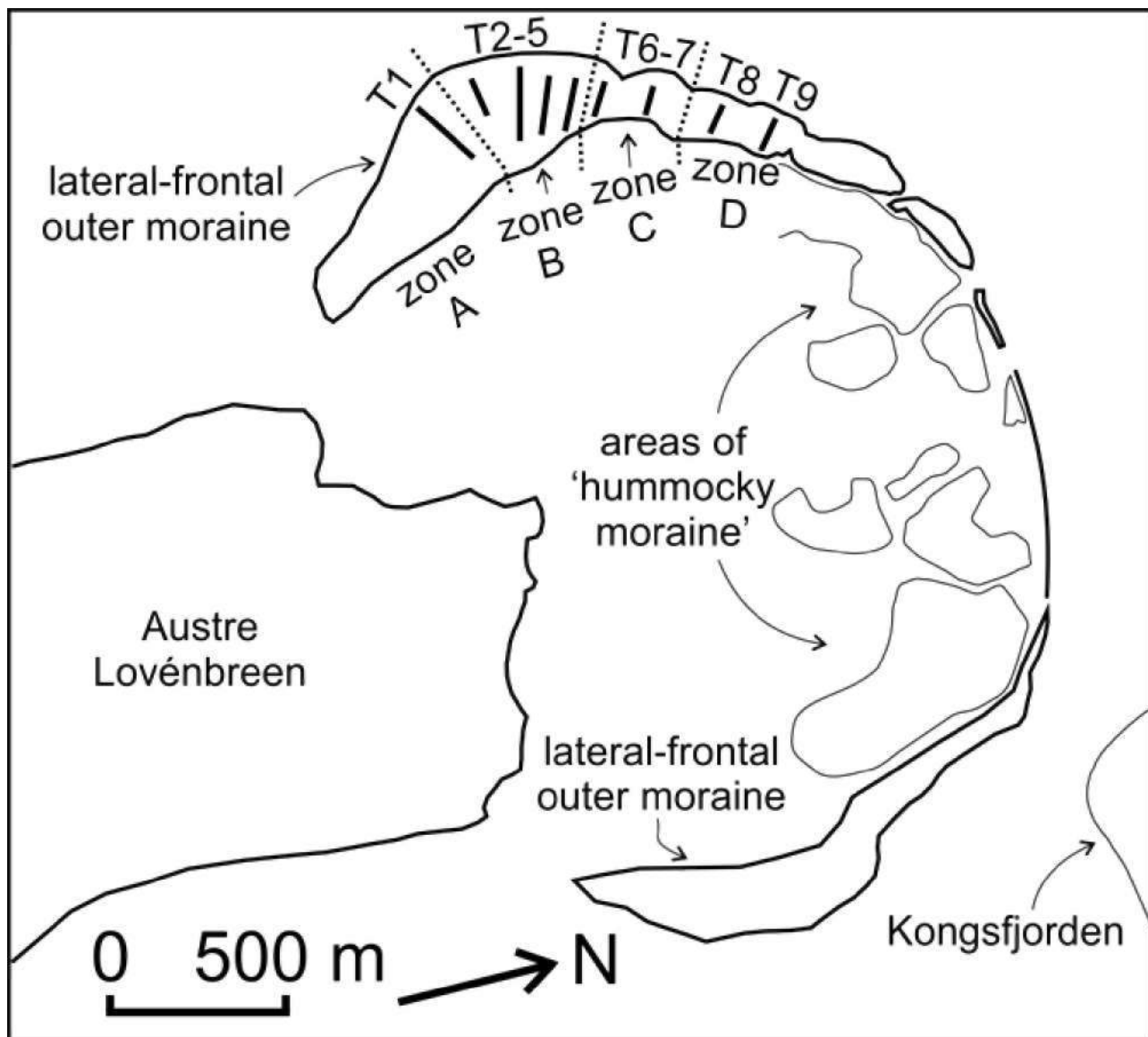
836



837 **Figure 2** (A) Aerial image of the terminus of Austre Lovénbreen (summer
838 2003) and the proglacial area; (B) outline of the Neoglacial lateral-frontal
839 moraine and the location of the GPR transects. Aerial image data from the UK
840 Natural Environment Research Council (NERC) Airborne Research and Survey
841 Facility (ARSF) are provided courtesy of NERC via the NERC Earth Observation
842 Data Centre (NEODC).

843

844
845
846
847
848
849
850
851
852
853
854
855



856 **Figure 2** (A) Aerial image of the terminus of Austre Lovénbreen (summer
857 2003) and the proglacial area; (B) outline of the Neoglacial lateral-frontal
858 moraine and the location of the GPR transects. Aerial image data from the UK
859 Natural Environment Research Council (NERC) Airborne Research and Survey
860 Facility (ARSF) are provided courtesy of NERC via the NERC Earth Observation
861 Data Centre (NEODC).

862

863

(A) 0

864

100

865

S, 200

866

A I 300

867

400

868

i i i i i i i

869

velocity (m ns¹)

870

87

(B) 0

87

100

87

S, 200

87

A I 300

87

400

87

i i i r i i

87

velocity (m ns¹)

87

879 **Figure 3** (A) Example common mid-point (CMP) survey across transect 2; (B)

880 CMP survey across transect 9.

881

882

883

884

885

886

887

888

889

890

891

892

893

894

895

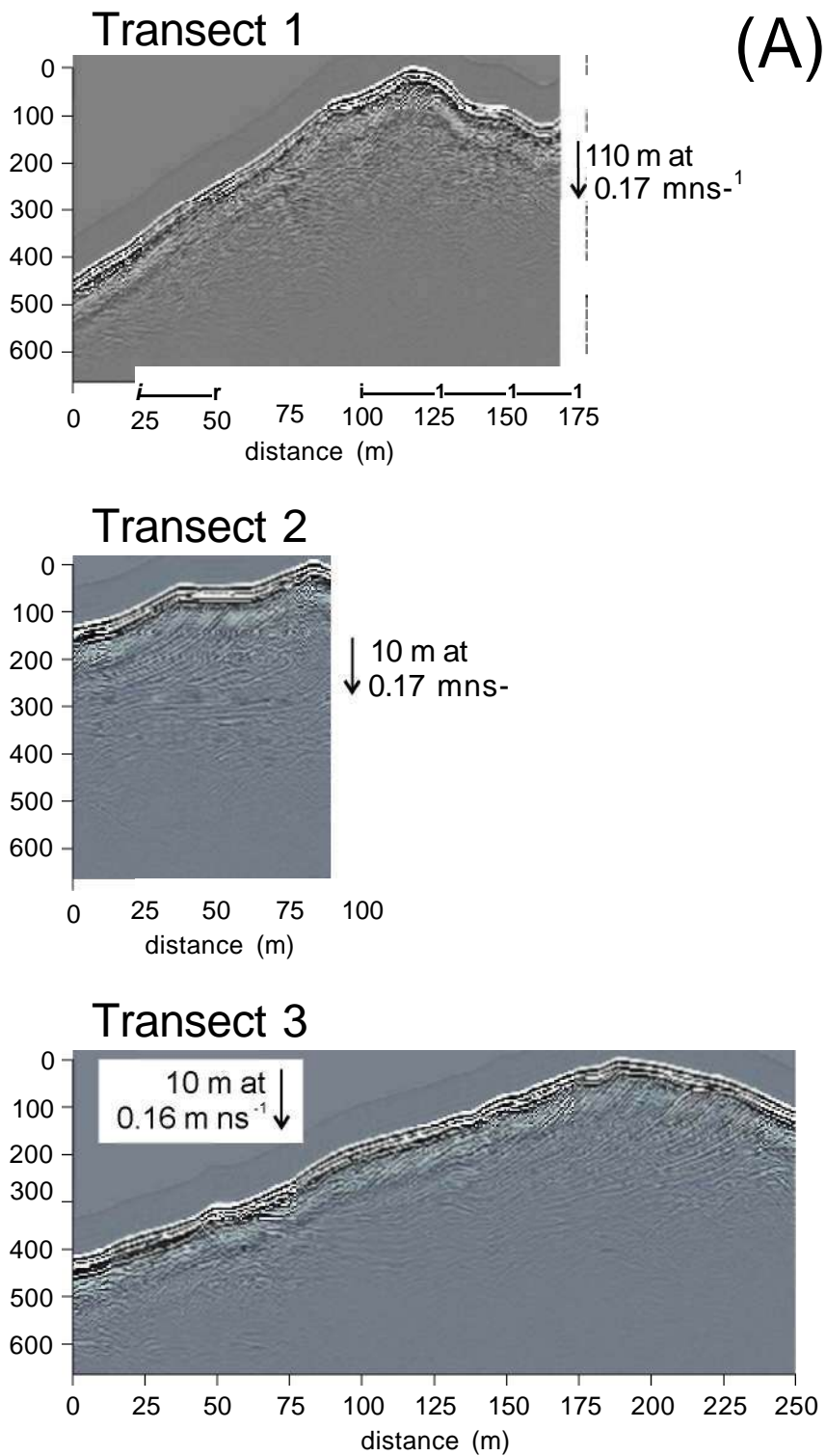
896

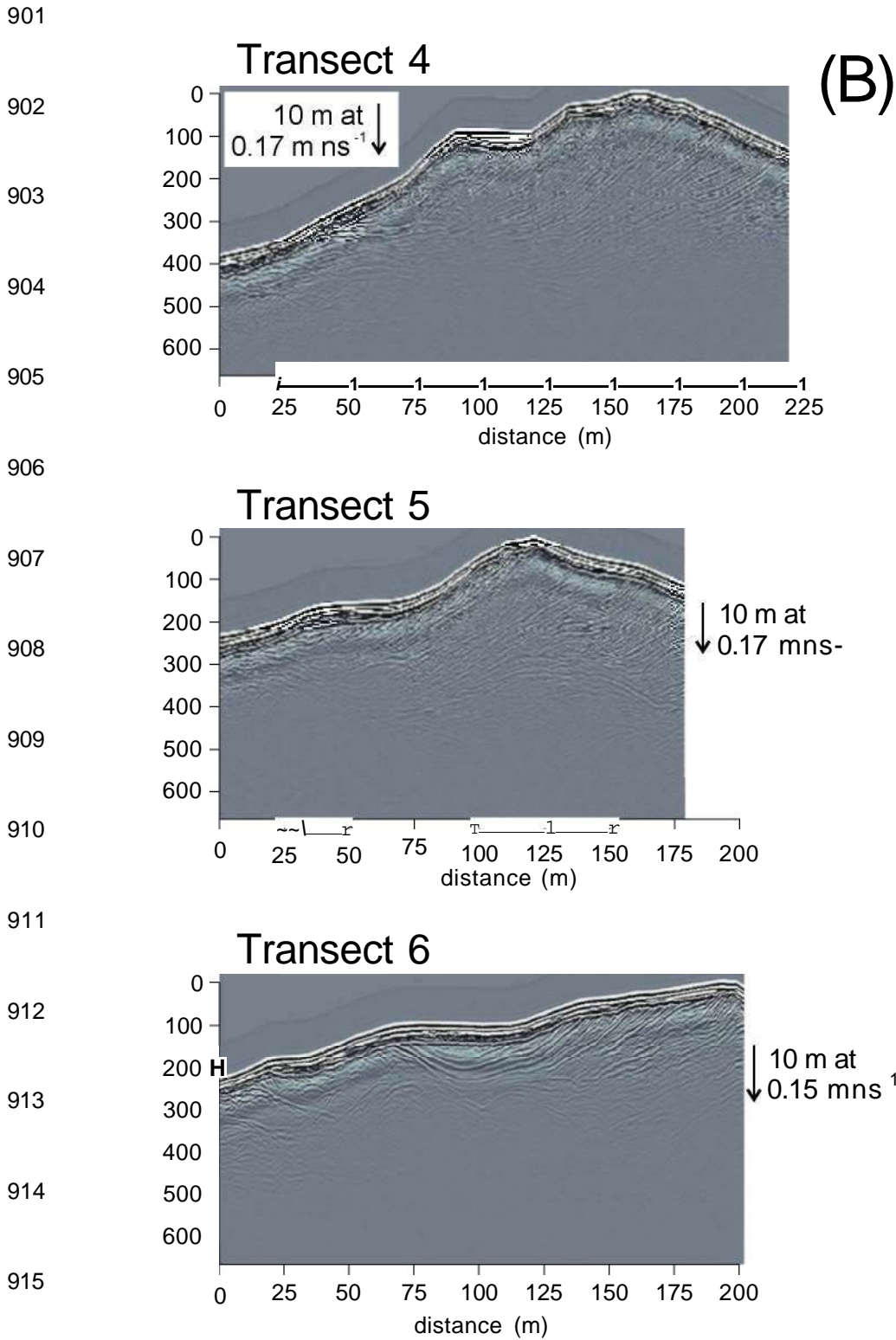
897

898 **Figure 4** Ground-penetrating radar (GPR) surveys as grey-scale images: (A)

899 transects 1–3; (B) transects 4–6; and (C) transects 7–9.

900

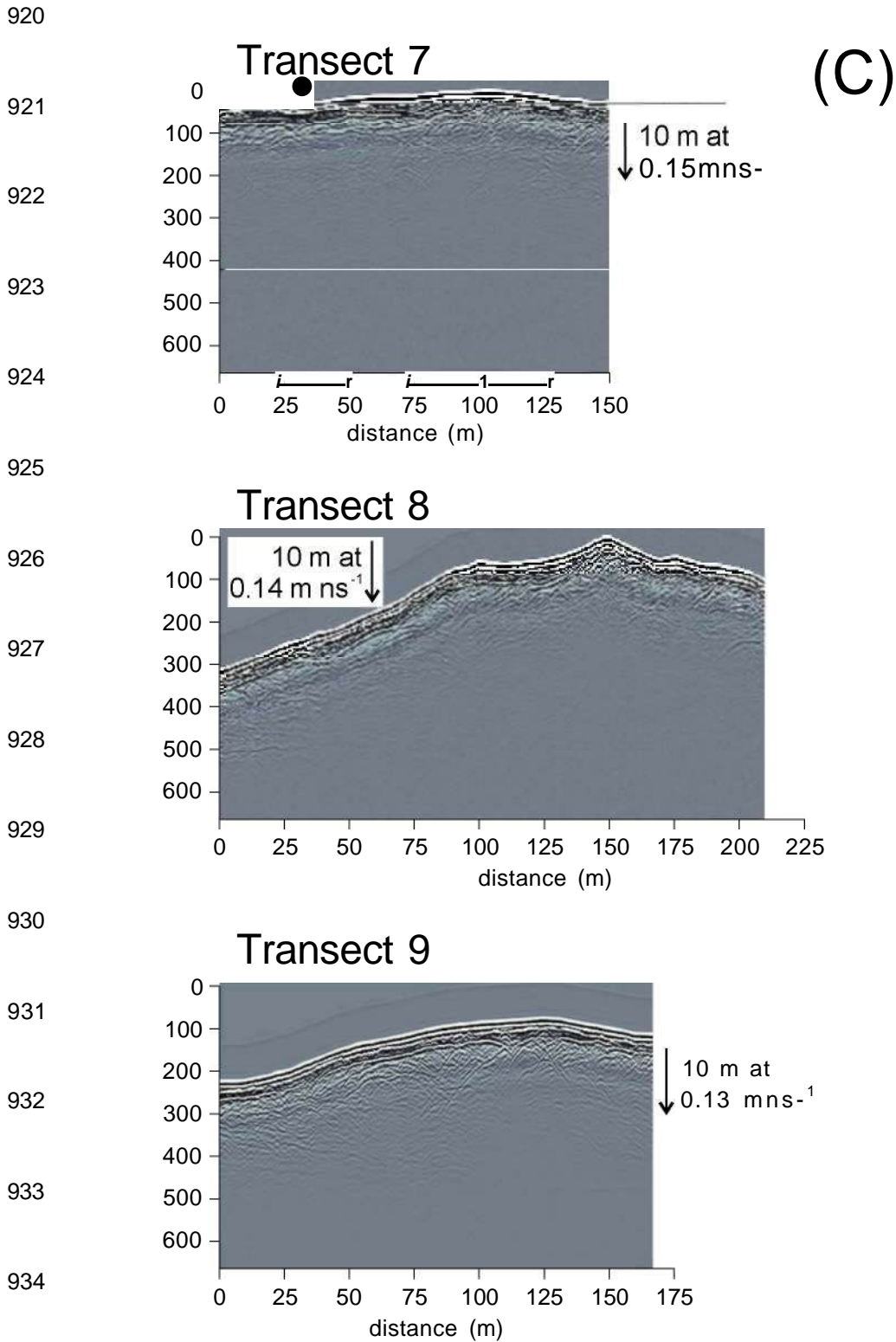




917 **Figure 4** Ground-penetrating radar (GPR) surveys as grey-scale images: (A)

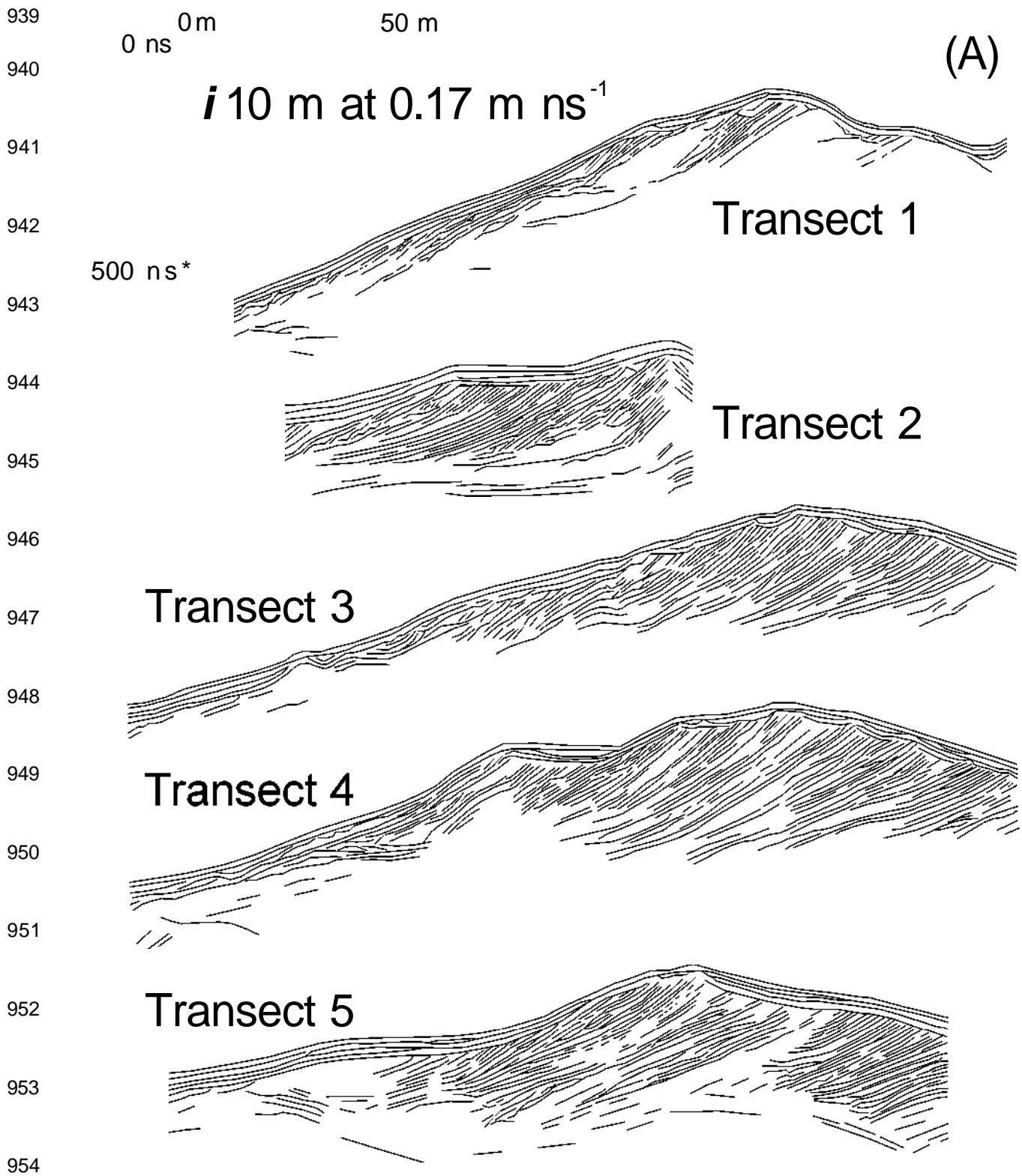
918 transects 1–3; (B) transects 4–6; and (C) transects 7–9.

919



936 **Figure 4** Ground-penetrating radar (GPR) surveys as grey-scale images: (A)

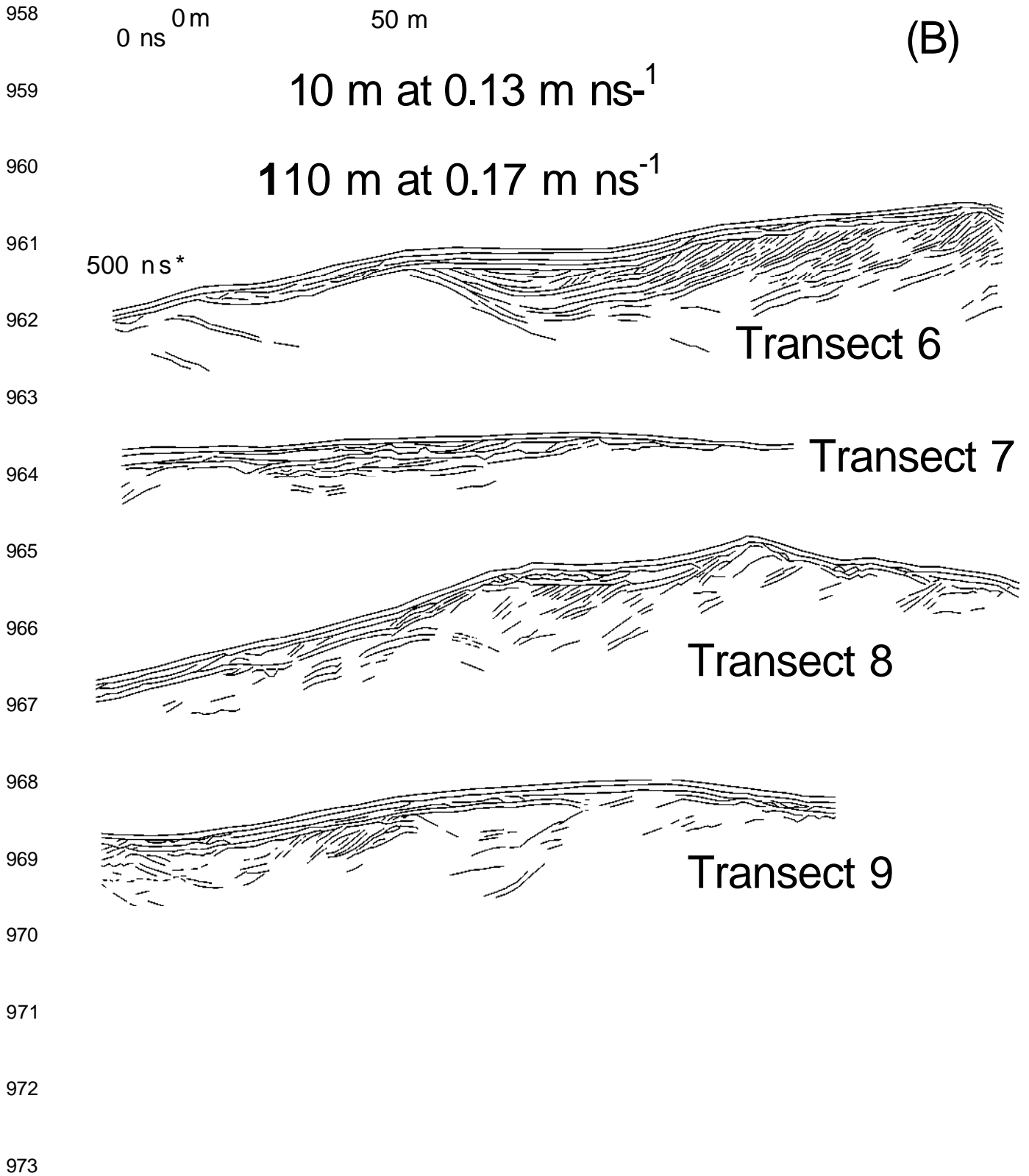
937 transects 1–3; (B) transects 4–6; and (C) transects 7–9.



955 **Figure 5** Key reflection characteristics of ground-penetrating radar (GPR)

956 surveys from transects 1–5 (A) and transects 6–9 (B).

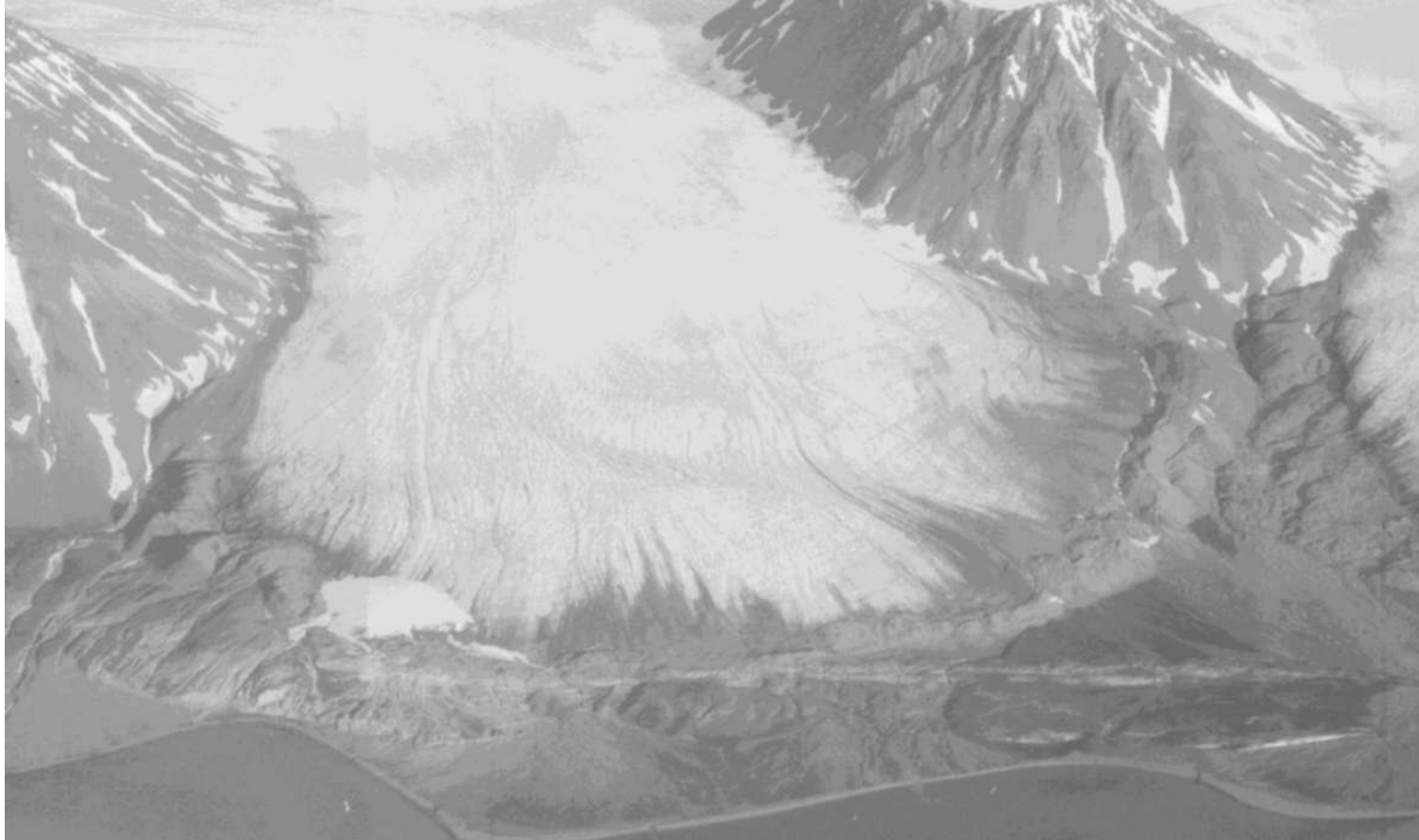
957



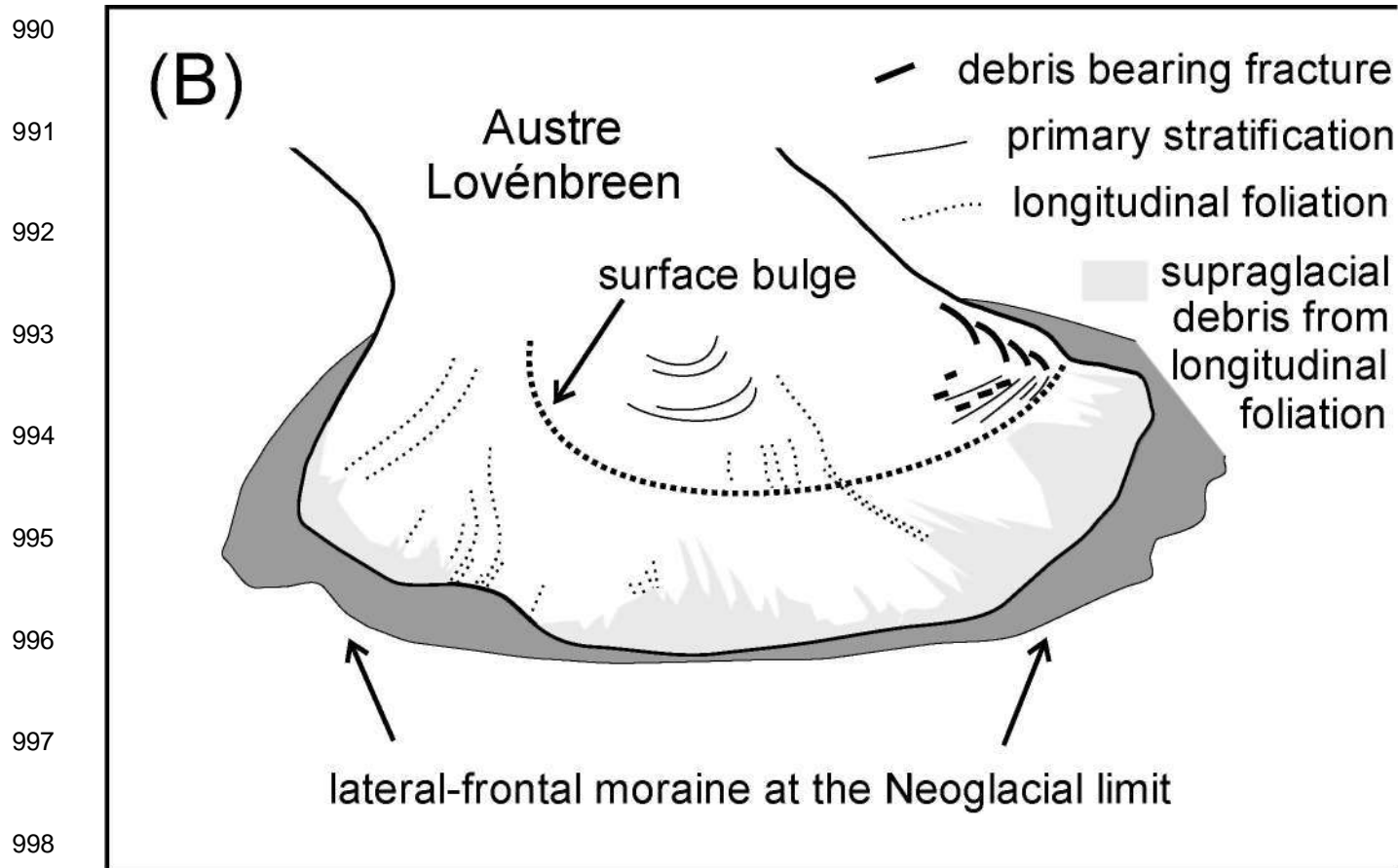
974 **Figure 5** Key reflection characteristics of ground-penetrating radar (GPR)

975 surveys from transects 1–5 (A) and transects 6–9 (B).

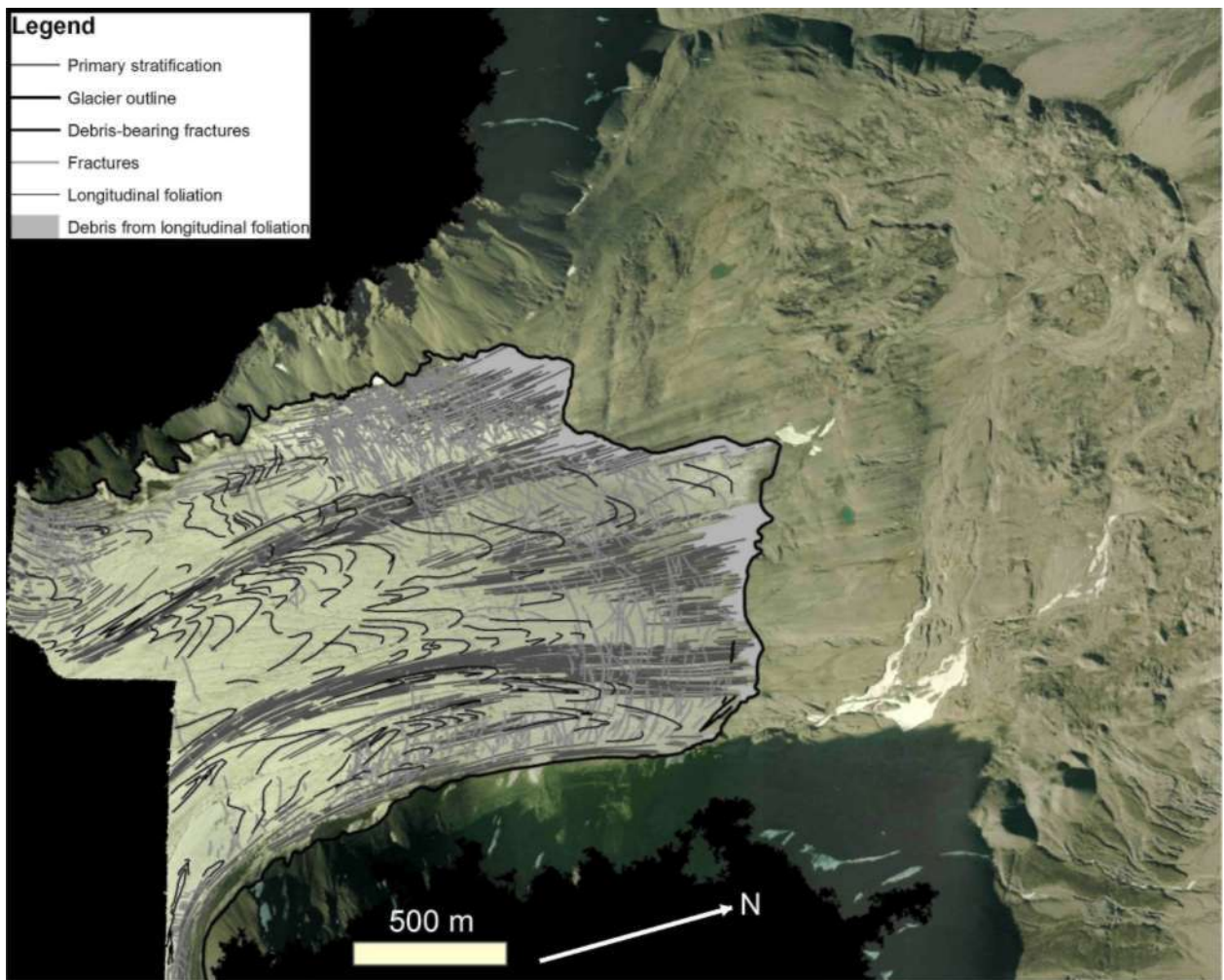
977
978
979
980
981
982
983
984
985



986 **Figure 6** (A) Oblique aerial image of the terminus of Austre Lovénbreen from 1936 imagery (part of aerial photograph
987 S36 1553, published with permission of the Norsk Polarinstitut); (B) Structural interpretation of Austre Lovénbreen in
988 1936. The scale varies across the image and associated interpretation, but the widest part of the glacier terminus is
989 around 1.4 km across.



999 **Figure 6** (A) Oblique aerial image of the terminus of Austre Lovénbreen from 1936 imagery (part of aerial photograph
 1000 S36 1553, published with permission of the Norsk Polarinstitut); (B) Structural interpretation of Austre Lovénbreen in
 1001 1936. The scale varies across the image and associated interpretation, but the widest part of the glacier terminus is
 1002 around 1.4 km across.



1014

1015 **Figure 7** Structural interpretation of Austre Lovénbreen from 2003 imagery.
 1016 Aerial image data from the UK Natural Environment Research Council (NERC)
 1017 Airborne Research and Survey Facility (ARSF) are provided courtesy of NERC
 1018 via the NERC Earth Observation Data Centre (NEODC).